JOURNAL OF CATALYSIS 151, 75–92 (1995)

Adsorption and Reactivity of NO on Copper-on-Alumina Catalysts

I. Formation of Nitrate Species and Their Influence on Reactivity in NO and NH_3 Conversion

Gabriele Centi,* Siglinda Perathoner,* Daniele Biglino,† and Elio Giamello†

*Department of Industrial Chemistry and Materials, University of Bologna, Viale Risorgimento 4, 40136 Bologna, Italy; and †Department of Inorganic Chemistry, Physical Chemistry and Materials, University of Turin, Via P. Giuria 9, 10125 Turin, Italy

Received April 21, 1994; revised September 1, 1994

The reactivity of copper-on-alumina catalysts in the reduction of NO by $NH_3 + O_2$ (SCR reaction) and oxidation of NH_3 to N_2 (NH_3ox reaction) as a function of the copper loading shows that (i) the specific rate of the SCR reaction per mole of copper decreases with increasing copper loading, whereas the NH_3ox reaction rate is nearly independent of the copper loading and (ii) the rate of the NH_3ox reaction is significantly higher in the absence of NO than that of the same reaction occurring during the SCR reaction. The catalysts were characterized by electron spin resonance (ESR), X-ray diffraction analysis, and UV–visible diffuse reflectance. The nature of the NO and NH_3 adsorbed species was studied using ESR and infrared (IR) spectroscopies, and IR studies of the reactive coadsorption of NO and NH_3 were carried out. The results obtained indicate that the above catalytic effects are due to the formation of nitrate species which block the reactivity of copper sites. The transformation of NO to N_2 via the intermediate formation of ammonium nitrate was shown, but the data suggest that this is only a secondary pathway of reaction responsible for the formation of N_2O as a byproduct. The nature of active copper species on the surface and the presence of competitive pathways of transformation of NO to N_2 are also discussed.

INTRODUCTION

Copper-based catalysts show a high activity in the conversion of nitrogen oxides to N_2 in several useful applications such as (i) the simultaneous removal of NO and SO_2 from flue gas, (ii) the catalytic direct decomposition of NO or its reduction in the presence of hydrocarbons, and (iii) the catalytic reduction of N_2O to N_2 (1–8). In recent years most of the research interest has been focused on the use of Cu-zeolites (Cu–ZSM-5, in particular) for these reactions due to their higher activity with respect to copper oxide supported on oxides such as Al_2O_3, SiO_2, ZrO_2, or TiO_2. However, the cost of synthesis of Cu-ZSM-5, for example, is around 25–30 times higher than that of CuO/Al_2O_3. Furthermore, for the former catalyst it is much more difficult to obtain the properties required for industrial development (e.g., suitable mechanical strength). For these reasons it was considered worthwhile to carry out an investigation on the reactivity in NO conversion of catalysts based on copper oxide supported on high-surface-area oxides, to obtain a better understanding of the reactivity of these catalysts in the reduction of NO to N_2 and consequently to learn more about the possibilities of tuning and improving their catalytic behavior. In addition, in some applications such as the reduction of NO by NH_3/O_2 (SCR) with simultaneous oxidation–adsorption of SO_2, supported CuO catalysts are preferable to Cu-zeolites.

In the process of combined removal of SO_2 and NO (6, 9) copper-on-alumina shows the best properties in comparison with other copper-based samples. However, an improvement in their SCR activity during the simultaneous conversion of SO_2 may be useful to reduce some drawbacks of these systems such as the formation of small amounts of N_2O (on the order of 20–40 ppm) and the formation of ammonium bisulfate during the catalytic reaction (6, 9). This requires a better understanding of the mechanism of interaction and surface conversion of NO species on copper-on-alumina.

These catalysts have been extensively characterized in the past. Strohmeier *et al.* (10) have studied the surface properties of a series of impregnated copper-on-alumina catalysts using various techniques concluding that the surface characteristics are affected by both metal loading and calcination temperature. At low loading (lower than around 4 wt.% of CuO for an alumina with a surface area of 100 $m^2\ g^{-1}$) and low calcination temperature (around 500–600°C) a defective spinel-type surface species ($CuAl_2O_4$) forms with most of the Cu^{2+} ions in a distorted octahedral geometry, unlike bulk $CuAl_2O_4$ in which about 60% of the copper ions have tetrahedral coordination and 40% octahedral coordination. At higher metal loadings, segregation of bulk-like CuO may also occur, characterized by copper ions in distorted tetrahedral coordination.

0021-9517/95 $6.00

Bulk-like $CuAl_2O_4$ forms for high calcination temperatures (about 900°C). Several authors agree on these conclusions regarding the surface structure of copper-on-alumina catalysts (11–18).

The interaction of NO on these catalysts, especially with reference to their behavior in the presence of CO, has been studied by infrared (IR) (19, 20) and ESR (21, 22) spectroscopies, by adsorption isotherms (23) and combined IR and thermal desorption (TDS) methods (24). Based on IR spectroscopy data, Fu *et al.* (19) reported the formation of two nitrosyl species assigned to interaction with Cu^{2+} ions of CuO (1888 cm^{-1}) and Cu^{2+} ions on the surface of the spinel $CuAl_2O_4$ (1862 cm^{-1}). Davydov (20), however, reports different frequencies for NO adsorbed on these catalysts, even though he also found differences depending on the copper loading on the alumina. In addition, Davydov also points out that different spectra are obtained for reduced and oxidized copper ions (20). ESR data (22) indicate the formation of a diamagnetic nitrosyl complex by reaction of NO with Cu^{2+}, in agreement with the results of Deen *et al.* (21) who used ESR spectroscopy to study the rate of reoxidation of reduced copper ions with NO. Adsorption isotherms (23), on the other hand, indicate that oxidized cupric surface ions chemisorb NO much faster than the cuprous ions, probably due to the presence of an orbital with an unpaired electron in Cu^{2+} ions (d^9) that is not present in Cu^+ ions (d^{10}). Hierl *et al.* (24) observed that on reduced copper ions, in addition to dissociative chemisorption of NO and formation of N_2, N_2O evolution also occurs via reaction of NO with adsorbed N atoms generated in the dissociative chemisorption step. On an oxidized surface NO coordinates on Cu^{2+} sites to form a Cu^{2+}–NO surface complex which can be further converted to nitrito complexes. These decompose in the temperature range 280–330°C with evolution of NO and formation of nitrato complexes. The latter finally decompose at higher temperatures with evolution of NO and O_2. On Cu^+ sites NO adsorption occurs in the form of a dinitrosyl complex which decomposes, forming N_2O and a $Cu^+(O)$ species which subsequently react with an NO molecule to form a surface nitrito complex. A dinitrosyl species, however, was not observed on copper-on-alumina samples, differently from Cu–ZSM-5 (8). The surface reactions of NO and ammonia over unsupported CuO have been studied with an isotopic labeling technique (25). The authors observed a progressive reduction of CuO and a parallel change in distribution of products of reaction. Feeding a ^{14}NO and $^{15}NH_3$ mixture over fresh CuO, almost exclusively $N^{14}N^{15}$ forms, but as the reaction proceeded, $^{15}N^{14}NO$, $^{14}N_2$, and $^{14}N_2O$ also appear. The authors suggest that the mixed nitrogen derives from the surface reaction between dissociative chemisorbed ammonia (rate-determining step) and NO, whereas the other products form from a surface copper complex containing two NO molecules which requires reduced copper ions.

Therefore, good agreement is found in the literature regarding the surface characterization of copper species in copper-on-alumina samples, but agreement is lacking on the nature of the adsorbed nitrogen species, their reactivity, and the mechanism of transformation. In particular, limited information is available in the literature on the latter two aspects, but the results of Hierl *et al.* (24), for example, indicate that complex phenomena may occur.

The objective of the work reported here was to study the reactivity of copper-on-alumina samples combined with EPR and IR characterization of the interaction and surface transformation of NO in the presence or absence of O_2 and/or ammonia. Copper-on-alumina samples with different degrees of copper loading were used in order to obtain a better understanding of the relationship between the nature of the copper species and adsorbed nitrogen oxide species and catalytic reactivity in NO conversion.

EXPERIMENTAL

Copper-on-alumina samples were prepared by an ion-exchange procedure using an aqueous ammoniacal 0.1 M $CuCl_2$ solution (sample with a copper content, expressed as CuO, of 0.1 wt%) or with an incipient wet impregnation method (other samples) using an aqueous copper acetate solution. In the latter case, due to the low solubility of copper acetate, the impregnation was repeated several times until the required copper loading was achieved with an intermediate stage of drying at 110°C. The so impregnated samples were dried overnight, calcined for 24 h at 350°C, and then heated for additional 8 h at 450°C in three steps with intermediate mixing and grinding of the material in order to obtain homogeneous samples. The final copper content in the sample was verified by chemical analysis. The homogeneity of copper content between the various grains and within the grains was then further checked using a scanning electron microscope equipped with X-ray microprobe analysis for the mapping of copper distribution. The alumina used for the preparation was a commercial γ-Al_2O_3 sample from Rhone–Poulenc (RP535A) with a surface area of 117 m^2g^{-1}. The surface area did not change significantly after copper addition and the porosity of the sample also remained unchanged. Before the addition of copper, the alumina pellets were ground to grain size in the 0.1–0.2-mm diameter range and used in this form for the catalytic tests.

Hereinafter, the copper-on-alumina samples will be designated as CuAl-x, where the index x represents the copper content in the sample in wt% expressed as CuO. The code number CuAl-5, for example, indicates a copper-on-alumina sample with a copper content of 5 wt% expressed as CuO.

Catalytic tests were carried out at atmospheric pressure in a quartz flow microreactor using 0.15 g of catalyst. The usual experimental tests were made to verify the absence in our experimental conditions of inter- and intraparticle diffusional limitations on the reaction rate. Due to the low concentration of reactants, temperature gradients within the pellets may be considered negligible, whereas the absence of an axial temperature profile was verified using an axial thermocouple sliding inside the catalytic bed. The inlet and outlet flow of the reactor were continuously monitored with an on-line VG SX200 mass quadrupole apparatus. All the lines from the reactor to the mass quadrupole detector were heated at 150°C in order to avoid the adsorption or condensation of reactants or reaction products. The feed mixture was prepared starting from already calibrated mixtures of the single reactants diluted in helium. The same mixtures were also used for the calibration of the mass quadrupole apparatus and for the periodic checking of instrument response. Fluctuations in the operating pressure of the mass quadrupole detector were compensated for, on the contrary, by using helium as an internal standard. The mass quadrupole data were transferred to a computer which elaborates the data before correcting the mass intensities to take into account the possible presence of multiple fragmentations. For example, 25% of the intensity of the mass at 18 (water) was subtracted from the mass at 17 (ammonia). Then, the mass intensities were converted to concentrations, conversion, and selectivity, and at the same time the N, O, and H balances were checked to ensure the correctness of the determinations.

Catalytic tests refer to the steady-state activity of samples usually attained after less than 1 h of time-on-stream. After attainment of the stationary condition, the activity behavior was continuously monitored for at least another hour checking that the activity/selectivity data do not change by more than the experimental error (about 6%).

X-band EPR spectra was recorded at 77 K and at room temperature on a Varian E-109 spectrometer equipped with a dual cavity and connected to a data station (STELAR, Italy) for data handling and elaboration. Varian pitch ($g = 2.0028$) was used as a reference for calibration of the g values. Nitric oxide and ammonia were purified by the freeze–pump–thaw technique before contact with the sample.

EPR spectra were recorded after standard treatment consisting in evacuation (1 h, $P = 10^{-4}$ Torr) at room temperature, 413, 573, 713, and 873 K respectively. To obtain samples in which either Cu^{2+} or Cu^{+} ions prevailed, the samples were submitted to standard procedures of oxidation or reduction. Oxidized samples were obtained by heating the dehydrated sample in an oxygen atmosphere for 1 h at 873 K, cooling to room temperature in oxygen, and when necessary removing the gas phase at the same temperature. Reduced samples were obtained by keeping the material at 713 K in a CO atmosphere for 15 h and removing the gas phase at the same temperature by direct pumping off.

Fourier-transform infrared (FT–IR) spectra (resolution 2 cm^{-1}) were recorded with a Perkin–Elmer 1750 instrument with a quartz cell (KBr windows) connected to grease-free evacuation and gas manipulation lines. The self-supporting disk technique was used. Before recording the spectra, the samples were evacuated at 500°C for 3 h or pretreated as follows. Oxygen (100 torr) was admitted to the sample (previously outgassed) at 500°C for 1 h. The sample was cooled to room temperature (RT) in an oxygen atmosphere, and O_2 was removed by evacuation at RT. This procedure was adopted in order to avoid the possible partial reduction of copper during the evacuation at higher temperature. The samples treated in this way are designated with the suffix oxidized.

X-ray diffraction (XRD) patterns were recorded with a Perkin–Elmer 1050/81 diffractometer using the powder technique and CuK_α radiation. For the quantification of the amount of crystalline CuO, 5 wt% of KBr was added as an internal standard and a mechanical mixture of 10% CuO and γ-Al_2O_3 was used as the reference. The ratio of the intensities of CuO and KBr was determined by estimating the area of the most intense diffraction peaks at $2\theta = 35.5°$ and 27° for CuO and KBr, respectively.

UV–visible diffuse reflectance spectra (UV–vis DRS) were recorded on a Kontron UVICON 860 instrument with barium sulfate as the reference sample. The spectra were recorded in air at room temperature and the data transformed according to the Kubelka–Munk equation:

$$f(R) = (1 - R_\infty)^2/2R_\infty. \quad [1]$$

RESULTS

Reactivity in a Flow Reactor

The effect of the reaction temperature on the conversion of NO and NH_3 on CuAl-5 is shown in Fig. 1a. The tests were carried out by adding ammonia in a stoichiometric amount according to

$$2\,NO + 2\,NH_3 + 0.5\,O_2 \rightarrow 2\,N_2 + 3\,H_2O. \quad [2]$$

Oxygen is in large excess with respect to the stoichiometric amount. This reaction is referred to as SCR. N_2 is the main product of reaction. A small formation of N_2O (around 10–20 ppm) was also detected, but the selectivities to N_2O were usually lower than 5–8%. For reaction temperatures higher than about 300°C the conversion of NO decreased slightly due to the competitive reaction of

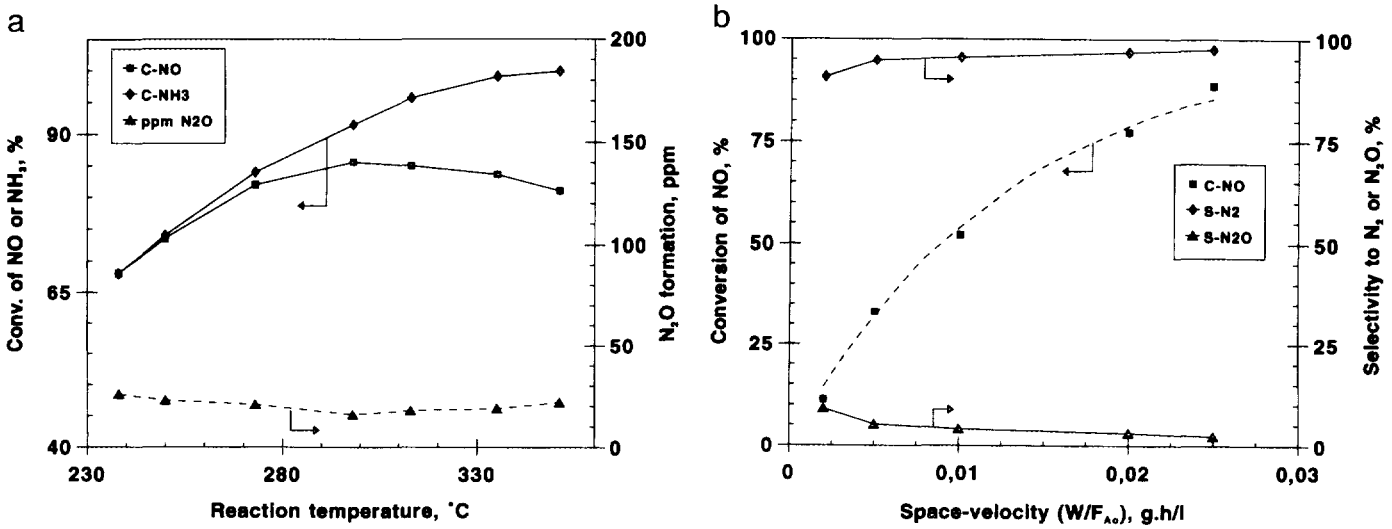

FIG. 1. (a) Conversion of NO and NH_3 in the reaction of NO + NH_3 + O_2 (SCR tests) as a function of the reaction temperature for CuAl-5. Experimental conditions: $W/F = 2.5 \times 10^{-2}$ g·h·liter^{-1}, 815 ppm NO, 818 ppm NH_3, 3% O_2 with the remainder being helium. (b) Conversion of NO and selectivity to N_2 and N_2O in SCR tests as a function of the space–velocity for CuAl-5. Experimental conditions as in Fig. 1a, temperature 300°C. The fit of the conversion from the space–velocity for a first-order rate equation is shown with a dotted line.

oxidation of NH_3 to N_2. The conversion of ammonia was, in fact, slightly higher than that of NO, especially for the higher temperatures. The relationship between catalytic reactivity and copper loading was therefore studied in the 250–300°C temperature range.

The dependence of the conversion of NO and selectivity to the products N_2 and N_2O on the space–velocity is shown in Fig. 1b. The conversion of NO increased with increasing space–velocity according to approximately a first-order rate of NO depletion. The selectivity to the two products, on the contrary, was nearly independent of the space–velocity; only a slight increase in the N_2O selectivity was noted for the shorter contact times. This indicates that N_2O is not the main reaction intermediate in the conversion of NO to N_2 in the presence of NH_3 + O_2.

The dependence of the conversion of NO and NH_3 at 250 and 300°C on the copper loading on alumina is shown in Figs. 2a and 2b, respectively. The selectivity to N_2O for all samples was around 5%, and decreased slightly with increasing copper content and increasing reaction temperature. No other by-products such as NO_2 were detected. For both reaction temperatures, the conversion of NO increased as a function of the copper loading. This shows the role of copper ions in the mechanism of NO transformation. The conversion of ammonia was slightly higher than that of NO, in particular for the higher temperature and copper loading, due to the presence of a side reaction of direct oxidation of ammonia to N_2.

In order to obtain a better understanding of the relative importance of this side reaction of ammonia conversion, catalytic tests were also carried out in which the feed contained only NH_3 + O_2. In these tests, summarized in Fig. 2 as a function of copper loading and reaction temperature, NO was absent. This reaction is referred to as NH_3ox. N_2 was the only product formed in the oxidation of ammonia at temperatures below 350°C, but small amounts of NO were also detected above this reaction temperature. For the higher copper loading and reaction temperature, the conversion of NH_3 to N_2 was higher than that expected on the basis of the following discussion. In fact, for a reaction temperature of 300°C and a copper loading of 10% for example, the conversion of NO was around 90% (see Fig. 2b) and the conversion of NH_3 in the same SCR tests, slightly higher (about 97%). Taking into account that NO and NH_3 were fed in a stoichiometric amount according to Eq. [2], the side reaction of direct ammonia conversion to N_2 must explain the difference between NH_3 and NO conversions in SCR tests and thus the extra 7% of ammonia conversion. A roughly similar conversion of NH_3 to N_2 was also expected in the tests without cofed NO (NH_3ox tests) assuming that additional factors do not modify the surface reactivity. However, the conversion observed was much higher (about 95% for a reaction temperature of 300°C and a copper loading of 10%; see Fig. 2b). This indicates that the rate of NH_3 conversion to N_2 without coadsorbed NO is much higher than in the presence of NO.

The dependence of the specific rate of NO depletion in SCR tests and of NH_3 depletion in NH_3ox tests on the copper loading and reaction temperature is reported in Fig. 3. The specific rate of reaction was determined as-

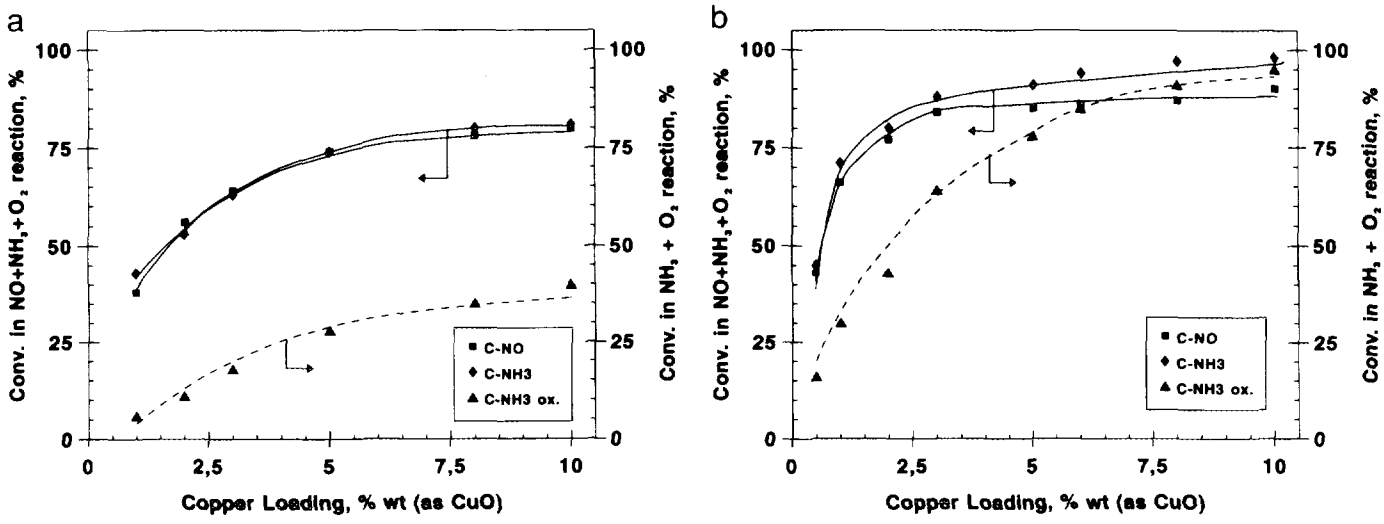

FIG. 2. Conversion of NO and NH_3 in the reaction of NO + NH_3 + O_2(SCR tests; see text) and conversion of NH_3 in the reaction of NH_3 + O_2(NH_3ox tests; see text) as a function of the copper content. Reaction temperature: 250°C (a) and 300°C (b); $W/F = 2.5 \times 10^{-2}$ g · h · liter^{-1}. Other experimental conditions: SCR 785 ppm NO, 791 ppm NH_3, 3% O_2 with the remainder being helium; NH_3ox 778 ppm NH_3, 3% O_2 with the remainder being helium.

suming a first-order rate equation for both reactions and a monodimensional plug-flow reactor model and dividing the rate constant determined in this way by the number of copper moles in the catalyst. Even though approximate, the first-order rate equation describes the reaction kinetics quite well in the range of interest for these tests (see Fig. 1b) and is in agreement with the results of kinetic studies on other active catalysts in SCR reactions (26). The general trend for the two reaction temperatures (250 and 300°C) is similar. While the specific rate per copper mole

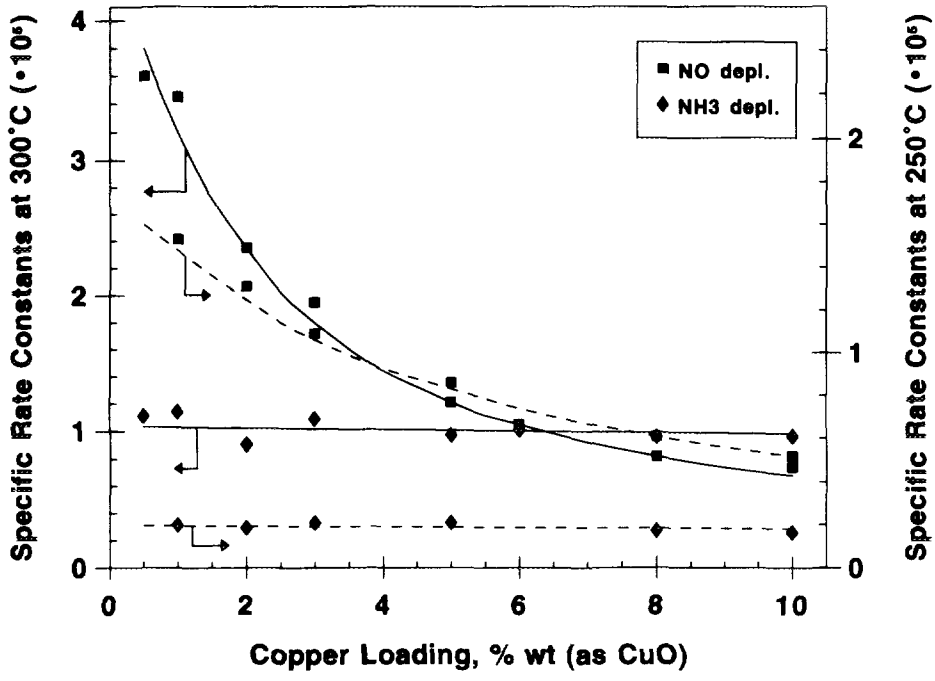

FIG. 3. Specific rate constant (liter · moles copper^{-1} · h^{-1}) for NO conversion in SCR tests and NH3 conversion in NH_3ox tests as a function of the copper loading and reaction temperature. Experimental conditions as in Fig. 2.

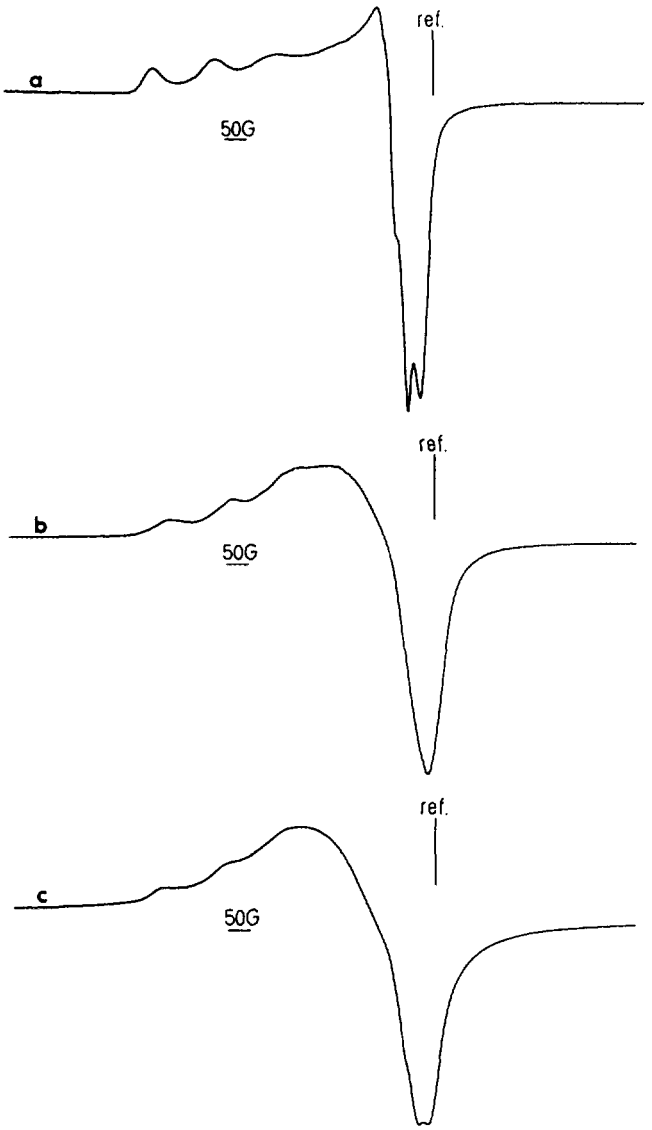

FIG. 4. EPR spectra at 77 K of CuAl-0.1 (a), CuAl-1 (b) and CuAl-5 (c) after outgassing at RT.

of the conversion of NH_3 to N_2 in NH_3ox tests is nearly independent of the copper loading, the specific rate of NO depletion decreased with increasing copper content in the catalyst.

EPR Characterization

The EPR spectra of copper-on-alumina samples outgassed at room temperature for 1 h are shown in Fig. 4. The spectra refer to CuAl-0.1, CuAl-1, and CuAl-6.3 samples, respectively. All spectra can be interpreted in terms of the overlap of, at least, two signals. The first one (signal A) is an axial signal with a resolved hyperfine structure visible in the parallel region and typical of Cu^{2+} containing systems. The second signal (signal B) is broad, unstructured and slightly axial. The spectra actually observed (Fig. 4) are partially resolved in the parallel region only. The resolution decreases with increasing copper content, i.e., from Figs. 4a to 4c.

The Hamiltonian spin parameters of signal A were evaluated on the basis of direct inspection of the spectrum and confirmed by a computer simulation. They are as follows:

$$g_{\parallel} = 2.323, \quad g_{\perp} = 2.060, \quad A_{\parallel} = 153\ \text{G}, \quad A_{\perp} \approx 20\text{–}25\ \text{G}.$$

The signal can be attributed to isolated or nearly isolated copper ions in axial symmetry (probably an axially distorted octahedral environment) and its parameters are close to those previously reported for copper-on-alumina systems (21, 27, 28).

Signal B can be assigned to interacting copper ions which are sufficiently close to one another to cause the smearing out of the hyperfine structure as a result of dipolar interaction.

Hereinafter these two species will be referred to as isolated and clustered copper ions. As the copper loading on the sample increases, the symmetry of the sites of isolated copper ions remains nearly unchanged, but the ratio between isolated and clustered species decreases. However, even for the sample with a very low copper content (0.1%, which corresponds to an amount around 100 times lower than that necessary to form a complete monolayer of copper oxide on the surface of the alumina used in this work) and prepared using a procedure that allows good dispersion of copper (ion exchange with Brønsted surface sites of alumina) the clustered copper species appears to be the more abundant one. Computer simulation of the experimental spectra (not reported for the sake of brevity) shows that in the case of CuAl-0.1 the clustered species (line width about 100 G) is about six times more abundant than the isolated one. This indicates that with increasing the copper loading there is not a progressive homogeneous distribution of copper ions on the surface of alumina with the formation of clustered copper species only for the higher copper loadings, but even for the lower surface copper contents the latter preferentially forms.

Thermovacuum treatments at increasing temperatures did not significantly change the spectra, but the overall intensity decreases. The intensity of EPR signals of CuAl-0.1 and CuAl-1 halves at 450°C and decreases to 1/10 of the original value at 600°C. The intensity of the EPR signal of CuAl-5 is less sensitive to the thermovacuum treatment; after evacuation at 600°C the intensity is still 2/3 of the intensity of the original signal of the sample evacuated at RT. The reduction in EPR signal intensity may be reasonably attributed to the reduction of Cu^{2+} to Cu^{+} suggesting that this process is easier for the samples with the lower copper content. No other copper species

were observed after thermovacuum treatment, but in CuAl-6 a second weak and unstructured signal due to isolated Cu^{2+} was present. The parameters of this second species, however, do not markedly differ from those reported above. The reduction of copper during the evacuation is confirmed by the EPR spectra of the samples consecutively reoxidized after this treatment. After reoxidation, in fact, the initial form and intensity of the spectra is restored, indicating that the reduction–reoxidation process is reversible and does not modify the nature of the copper species. The EPR spectra of the samples after the catalytic tests do not significantly differ from those discussed above.

The changes in the EPR signal upon admission of NO or NH_3 were studied on all the above samples and no significant differences between the samples were found. Since the spectra obtained for CuAl-0.1 were the clearest, only this sample will be discussed.

For the CuAl-0.1 sample after the reoxidation step and evacuation at room temperature to remove adsorbed oxygen, the spectrum reported in Fig. 5a is observed. Adsorption of NO at room temperature gives rise (spectrum 5b) to a slight decrease in the whole Cu^{2+} EPR signal (due to the formation of a diamagnetic Cu^{2+}–NO adduct as reported in Ref. 8) and, at the same time, to the appearance of a new signal at high field characterized by $g_{\parallel} = 1.95$ and $g_{\perp} = 1.99$. The latter signal is observed only at 77 K.

The above-reported g values (both lower than the free spin value 2.0023) suggest that the corresponding spectrum is due to the NO molecule adsorbed in molecular form on Al^{3+} ions. NO is an 11-electron π radical with one electron in the π antibonding orbitals: for this type of radical negative Δg_{ii} shift are expected ($\Delta g_{ii} = g_{ii} - g_e$). Furthermore, the signal observed at high field closely resembles the one recorded by Lunsford in the case of NO adsorption on bare alumina (29) in similar conditions of surface hydration. When the NO atmosphere is pumped off at room temperature the intensity of the Cu^{2+} signal grows and the original intensity of the starting spectrum (Fig. 5a) is nearly restored. The effect of NO adsorption on the oxidized samples, therefore, is the reversible formation of (i) diamagnetic mononitrosyls on cupric ions (observed in terms of intensity modifications of the Cu^{2+} signal) and (ii) a molecular adduct Al^{3+}–NO on the oxide matrix. The same experiment was carried out on various reduced samples mainly containing copper in the form of Cu^{+} ions. Except for the relative intensity of the two signals (Cu^{2+} and Al^{3+}–NO) the spectra obtained were the same as reported in Fig. 5b. This indicates that mononitrosylic adducts on Cu^{+} do not form on both oxidized and reduced samples. A paramagnetic nitrosylic adduct has, in fact, been observed in the case of cuprous ions on silica and in zeolite systems. This adduct is formed by

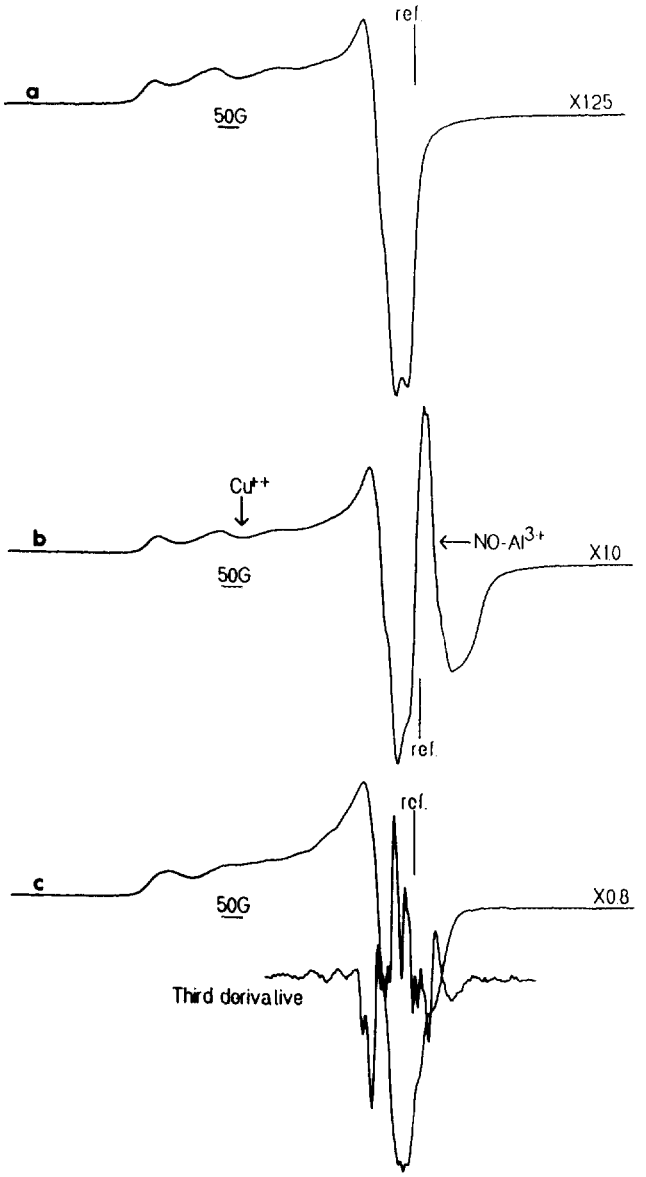

FIG. 5. EPR spectra at 77 K of CuAl-0.1, evacuated at 600°C, then reoxidized for 1 h with 115 Torr of O_2 at 600°C and subsequently evacuated at RT to remove gaseous oxygen (a), of sample (a) after consecutive adsorption of NO (20 torr at RT) (b), and of sample (a) after consecutive adsorption of NH_3 (20 torr at RT) (c). In this spectrum the third derivative profile overlaps the first derivative profile.

interaction of NO with Cu^{+} ions and is characterized by a wide and well-resolved hyperfine structure due to the interaction of the copper nucleus with the unpaired electron (8, 30–32).

The EPR spectrum of CuAl-0.1 after adsorption of NH_3 at room temperature is also shown in Fig. 5 (spectrum 5c). Ammonia interacts with Cu^{2+} ions perturbing the perpendicular component of the signal which significantly broadens. This is due both to the onset of new species with

distinct g values and to the superhyperfine interaction between the nucleus of nitrogen and the unpaired electron of the Cu^{2+} ion. This interaction leads to the splitting of the perpendicular component of the isolated Cu^{2+} ion signal, which is not fully resolved but which can be better appreciated in the third derivative profile of the central part of the spectrum also reported in Fig. 5c. The spectral shape is in agreement with the formation of copper–ammonia complexes (33) probably with one and two NH_3 ligands as confirmed by preliminary computer simulations. Similar complexes have been evidenced for copper ions in a zeolitic matrix (34, 35). No evidence was obtained from EPR about the interaction (if any) of NH_3 with clustered Cu^{2+} ions.

Infrared Spectra

a. Ammonia adsorption. The nature of adsorbed species formed by adsorption of ammonia on CuAl-5 and their reactivity with O_2 at 300°C (spectra d–f) is compared in Fig. 6A with that on the alumina support (spectra a–c). Both catalysts were preactivated under vacuum at 500°C to remove water and other adsorbed species; however, small amounts of water were fed together with ammonia as shown by the band at 1635 cm^{-1} (spectrum a of Fig. 6A) of ammonia in contact with the catalyst. This makes it possible to create Brønsted sites on the surface and thus to have a more significant analysis of the nature of the adsorbed species, since water is always present during the catalytic reaction. Adsorbed water, however, can be easily removed by a brief evacuation (see spectrum b of Fig. 6A).

Ammonia chemisorbs on the alumina support in the form of ammonium ions (1450 cm^{-1} and a weak shoulder at 1680 cm^{-1}) by reaction with the surface Brønsted acidic sites of alumina and as coordinated ammonia on surface Lewis sites (1612 and 1252 cm^{-1}, δ_{as} and δ_s, respectively), in good agreement with literature data (36). Correspondingly, the bands in the OH stretching region [3775, 3730, and 3680 cm^{-1}; type I, II, and III OH groups according to the Knözinger–Ratnasamy classification (37)] disappear with formation of a broad intense absorption band centered at 3160 cm^{-1}, with poorly resolved bands at 3380 and 3530 cm^{-1}, in agreement with that expected for coordinated ammonia and ammonium ions.

In addition to the above species, a shoulder is observed at about 1500 cm^{-1} which may suggest the formation of NH_2 groups coordinated to Al (38) (spectrum b of Fig. 6A), but the latter species readily disappear in the presence of O_2 (spectrum c of Fig. 6A). Apparently, the other ammonia chemisorbed species react slowly with O_2 and especially ammonium ions disappear at a lower rate in comparison with coordinated ammonia, as deduced from the change in their relative intensities. It should be noted, however, that water is produced in the oxidation of chemisorbed ammonia and new Brønsted sites may be created on the surface of alumina and coordinated ammonia may shift to Brønsted sites forming a more stable complex. Under vacuum, on the contrary, all the above chemisorbed ammonia species are rather stable at 300°C.

Similar chemisorbed ammonia species are detected on CuAl-5 (spectrum d of Fig. 6A), but the intensity of the ammonium ion is relatively less intense. Free OH groups in the 3000–4000 cm^{-1} region are not detected for CuAl-5 indicating that Brønsted sites which were present for alumina alone had reacted with copper ions.

In contact with O_2 at 300°C (spectra e and f of Fig. 6A), all chemisorbed ammonia species very quickly disappear. After 20 min in contact with O_2, only a broad band at 1635 cm^{-1} is found, presumably due to the water formed during the oxidation of chemisorbed ammonia. In comparison with pure alumina, the oxidation of ammonia is much more rapid, evidencing the catalytic effect of copper ions in this reaction.

The spectra of adsorbed ammonia species formed in the interaction with CuAl-1 and CuAl-10 is shown in Fig. 6B. For both catalysts after evacuation at 500°C, no free OH groups are observed in the 3000–4000 cm^{-1} range indicating the complete reaction with copper ions, even for the sample with the lower copper content. The spectrum obtained by ammonia adsorption on both these catalysts is relatively similar to that obtained on CuAl-5. In all cases, coordinated ammonia is the more intense species and the intensity of the ammonium ion is rather weak. In CuAl-10 and possibly in CuAl-1 a band is observed at 1500 cm^{-1} especially after evacuation at 200°C (spectrum d of Fig. 6B), but due to the low amount of surface alumina sites in this sample with a copper loading higher than the monolayer capacity, it seems more reasonable to attribute this band to slightly positively charged coordinated ammonia on Cu^{2+} sites, according to Jobson *et al.* (39). For this species a second weak band is expected at around 1600 cm^{-1}, in agreement with the weak shoulder observed in spectrum d of Fig. 6B, where this species is rather intense. Interestingly, after evacuation at 200°C on CuAl-10, an additional weak band centered at 1560 cm^{-1} forms (spectrum d of Fig. 6B), possibly due to the formation of a $(NH_2)^-$ group (36, 40) due to the heterolytic dissociation of ammonia.

b. NO adsorption. The infrared spectra of NO adsorption on alumina, CuAl-5, CuAl-1, and CuAl-10 are reported in Fig. 7A–7D respectively. For comparison, the spectrum of NO adsorbed on a reference sample of bulk $CuAl_2O_4$ is also reported in Fig. 7C (spectrum d). Samples, unless otherwise indicated, were activated under vacuum for 3 h at 500°C. NO was kept in contact with the samples at 300°C, because differently from the case of ammonia adsorption, the nature of nitrogen oxide chemisorbed spe-

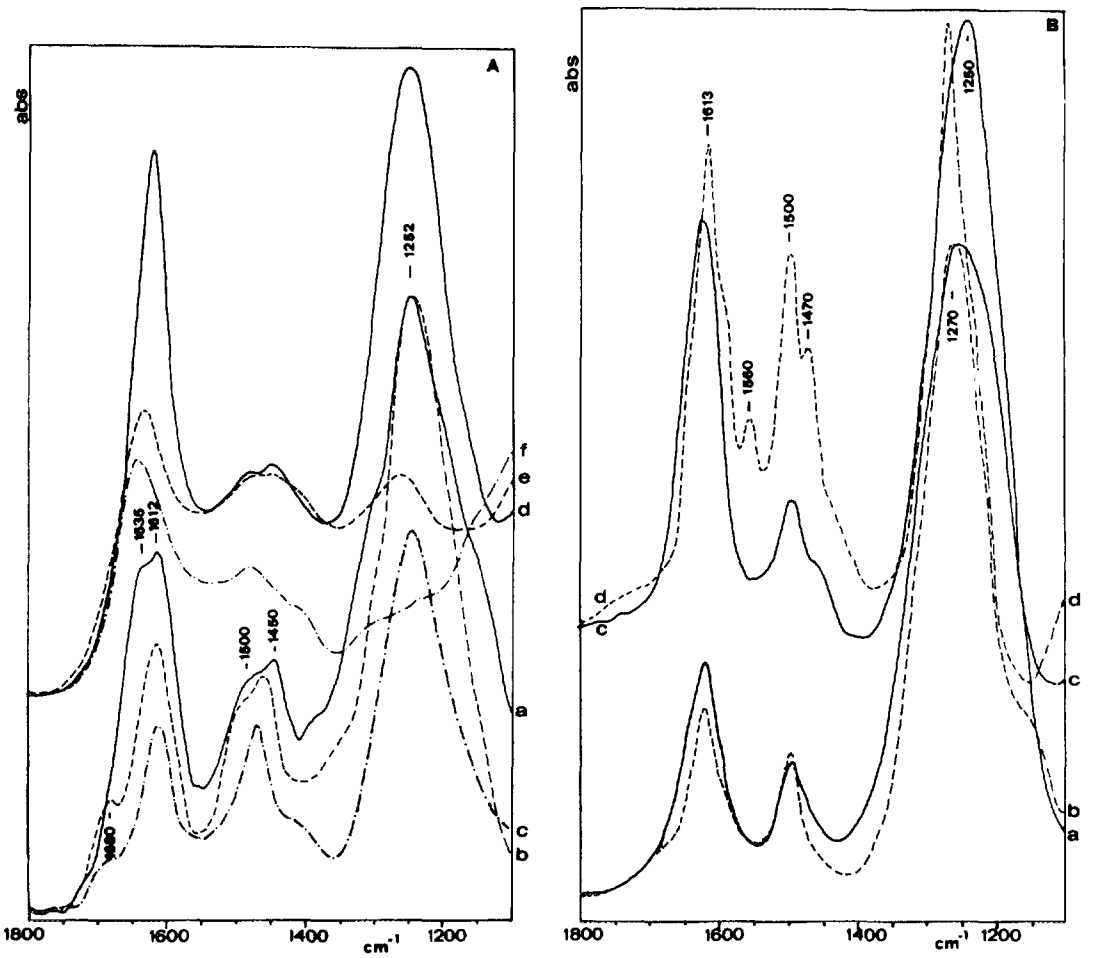

FIG. 6. Infrared spectra of ammonia adsorbed on a γ-Al_2O_3 support (spectra a–c of A), on CuAl-5 (spectra d–f of A), on CuAl-1 (spectra a and b of B) and on CuAl-10 (spectra c and d of B). All samples were evacuated at 500°C before adsorption of ammonia (40 torr). (A) Al_2O_3, (a) RT adsorption, (b) subsequent evacuation at RT for 1 h, (c) after consecutive treatment with O_2 (60 Torr) at 300°C for 20 min. (A) CuAl-5, (d) adsorption of ammonia at RT and evacuation at RT for 1 h, (e) after consecutive contact with O_2 (60 Torr) at 300°C for 10 min and (f) for 20 min. (B) CuAl-1 (a) contact with ammonia at 100°C for 1 h and subsequent evacuation at RT for 1 h, (b) consecutive evacuation at 150°C for 10 min. (B) CuAl-10 (c) contact with ammonia at 100°C for 1 h and subsequent evacuation at RT for 1 h, (d) consecutive evacuation at 200°C for 10 min.

cies was found to depend considerably on the reaction temperature. The temperature of 300°C was thus chosen to be more representative of the nature of nitrogen oxide chemisorbed species present during the catalytic reaction. In addition, the infrared spectra of NO adsorbed at room or lower temperatures on copper catalysts have already been reported in the literature (19, 20 and references therein, 41), but the species formed by high temperature interaction or their change as a function of the copper loading on alumina were not studied. Spectra were usually recorded at room temperature in contact with NO (after subtraction of the contribution of gas phase species) and with subsequent evacuation at different times and temperatures. The reactivity of chemisorbed nitrogen-containing species with O_2 at 300°C was also studied.

Summarized in Fig. 7A are the spectra obtained for NO in contact with the alumina support at 300°C (spectrum a) and subsequent evacuation for 1 h (spectrum b). An intense band develops at 1236 cm^{-1} together with less intense bands at 1340, 1460, and 1562 cm^{-1}. No bands are present above 1700 cm^{-1}. When alumina after interaction with NO at 300°C and subsequent evacuation is put in contact with O_2 at 300°C (spectrum c of Fig. 7A), the more intense band shifts to 1250 cm^{-1} and the two bands at 1562 and 1460 cm^{-1} increase considerably in intensity. The single intense band at 1236 cm^{-1} may be attributed to a bridging Al–O–N–O–Al nitrite species (20), because for nitrite or nitrate species two bands are expected in the 1700–1200 cm^{-1} region with the more intense in the 1400–1600 cm^{-1} region. This species readily transforms to a bidentate nitrate ion (bands at 1562 and 1250 cm^{-1}) partially present also before interaction with O_2. The two

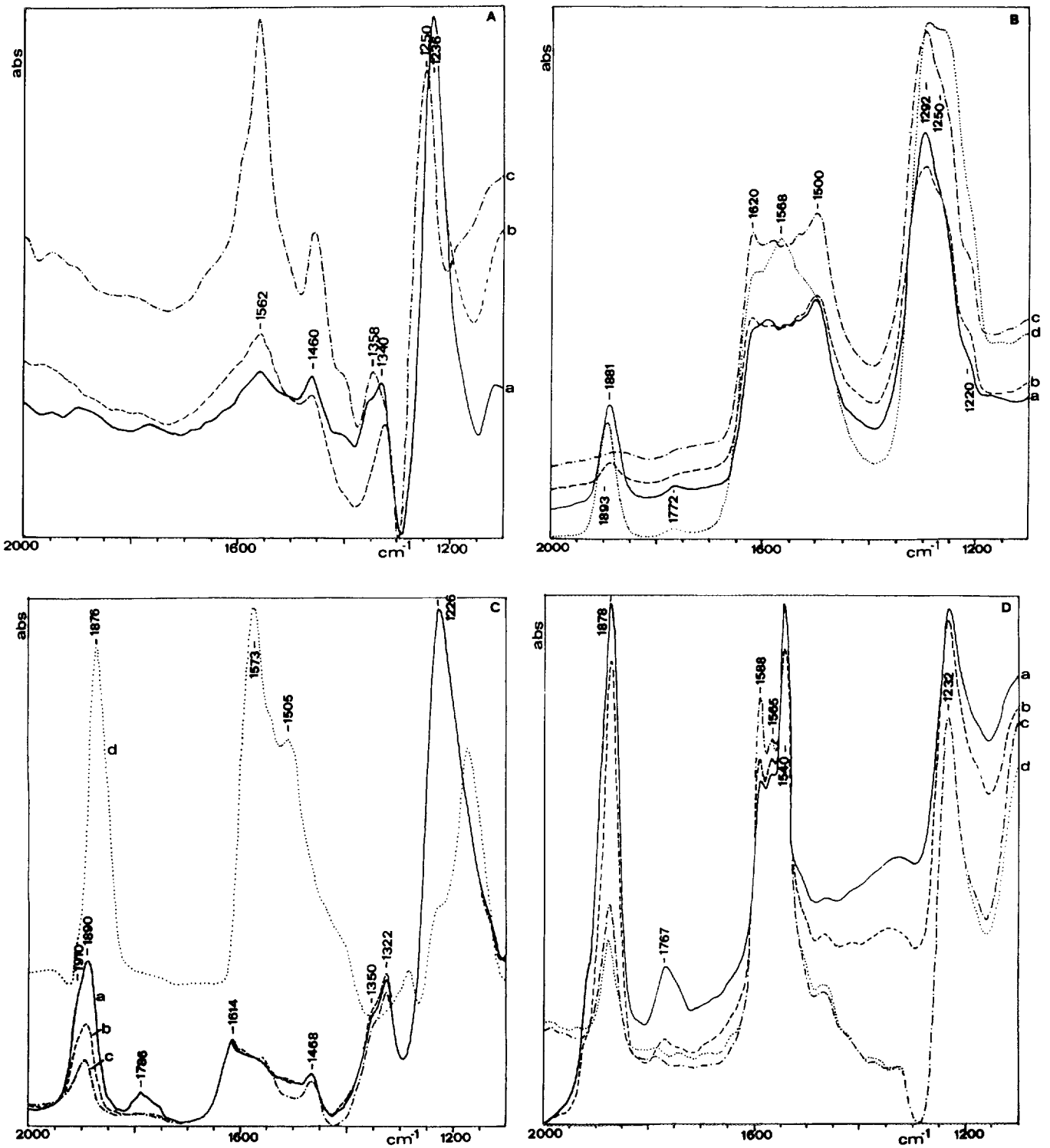

FIG. 7. Infrared spectra of NO adsorbed on a γ-Al_2O_3 support (A), on CuAl-5 (B), on CuAl-1 (spectra a–c of C), on CuAl-10 (D) and on a reference sample of bulk $CuAl_2O_4$ (spectrum d of C). All samples were evacuated at 500°C before adsorption of purified NO (40 Torr), unless otherwise specified (some spectra are shown for samples subjected to an oxidizing treatment with oxygen; see Experimental). (A) Al_2O_3 (a) contact at 300°C for 12 h, (b) subsequent evacuation for 1 h, (c) after consecutive treatment with O_2 (60 Torr) at 300°C for 20 min. (B) CuAl-5 (a) contact at 300°C for 2 h, (b) subsequent evacuation for 2 min and (c) for 30 min, (d) as for spectrum a, but on the oxidized sample. (C) CuAl-1 (a) contact at 300°C with NO for 2 h, (b) subsequent evacuation for 2 min and (c) for 12 min. (D) CuAl-10 (a) contact with NO at 300°C for 2 h, (b) subsequent evacuation for 2 min, (c) for 12 min and (d) for 22 min. (C) $CuAl_2O_4$ (d) contact with NO as for spectrum a of Fig. 7C.

weak bands at 1460 and about 1350 cm^{-1} may be attributed to a linearly coordinated nitrite ion.

When copper ions are present (Figs. 7B–7D) the nature of the adsorbed nitrogen oxide species changes significantly. An intense absorption band is found near 1880–1900 cm^{-1} in the samples in contact with NO at 300°C, which progressively disappears upon evacuation. In addition, a weak and rather broad band centered at about 1770–1780 cm^{-1} is also observed which disappears more quickly than the former upon evacuation (see spectra a–c in Figs. 7B–7D). The latter band can be attributed to a partially negative mononitrosyl species and the former to a partially positive mononitrosyl species (20). The frequency of the latter species is sensitive to the pretreatment of the catalyst before NO contact at 300°C. For example, on CuAl-5 the band is found at 1881 cm^{-1} when the pretreatment was evacuation at 500°C and at 1893 cm^{-1} when the sample after evacuation was put in contact with O_2 at 500°C, then cooled to RT in an oxygen atmosphere followed by removal of the gaseous and adsorbed oxygen by evacuation at this temperature. On CuY-zeolites, NO mononitrosyl species coordinated on Cu^{2+} are observed at 1900–1920 cm^{-1}, whereas coordination on Cu^+ ions formed by prereduction gives rise to a broad band at 1740–1750 cm^{-1} (20). On Cu-ZSM-5 a band at 1912 cm^{-1} for Cu^{2+}–NO and a second band at 1811 cm^{-1} Cu^+-NO have instead been reported (8). The shift of mononitrosyl to higher frequencies with respect to gaseous NO (1874 cm^{-1}) is due to the electron donation from π^*-orbitals of NO to empty *d*-orbitals of Cu^{2+} ions with a back-donation from the copper *d*-orbitals to the antibonding orbital of NO. A shift to lower frequencies than gaseous NO thus requires a net electron transfer to NO orbitals which in turn implies a reduced copper ion. The formation of metallic copper during vacuum treatment of $CuO–Al_2O_3$ is, on the other hand, very unlikely and never observed. The two bands at about 1880–1900 and 1760–1780 cm^{-1} can thus be attributed to mononitrosyl species coordinated on Cu^{2+} and Cu^+ ions, respectively, the latter probably formed during the oxidation of NO to nitrite–nitrate species or during pretreatment of the sample.

It should be noted that Cu^+–NO mononitrosyl species on isolated Cu^+ ions in ZSM-5 zeolite are clearly visible by IR (band at 1811 cm^{-1}) and EPR (8) spectroscopy. This species, however, can be detected only at 77 K; at room temperature it first transforms to a dinitrosyl species in the presence of NO and then oxidizes the copper to Cu^{2+}. EPR results on copper-on-alumina (Fig. 5) indicate the absence of formation of the Cu^+-NO species, but show only the formation of (i) a Cu^{2+}–NO nitrosyl (indicated by the lowering of intensity of the spectrum) and (ii) an Al^{3+}–NO adduct at 77 K that disappears at room temperature. Apparently, the IR and EPR results do not agree with regard to the formation of a Cu^+-NO nitrosyl species. Hierl *et al.* (24) also has reported the absence of formation of this species on copper-on-alumina. Our IR results regarding the interaction of NO at room temperature with the catalysts fail to detect the presence of such a species, detected, on the contrary, in the tests of NO interaction at 300°C (Fig. 7). We may conclude that this species on copper-on-alumina may be detected only under special conditions and reasonably forms in the oxidation of nitrogen oxide adspecies. The Cu^+-NO species, on the other hand, is rather unstable and rapidly disappears by evacuation in agreement with expectations (19). The slight shift from 1881 to 1893 cm^{-1} on CuAl-5 pretreated in vacuum or in an oxidizing atmosphere (compare spectra a and d of Fig. 7B) is thus probably due to an increased electron acceptor ability of copper ions after the oxidizing treatment, caused by the presence of coordinated oxygen species not completely removed after the RT evacuation. It should be pointed out that a weak band at 1360 cm^{-1} is noted on the catalyst after adsorption of oxygen only. This band is in agreement with the presence of an $(O_2)^{\delta-}$ species.

It is interesting to note that the position of the mononitrosyl species after similar pretreatments of the catalysts depends on the copper loading (compare spectra a of Figs. 7C, 7B, and 7D for samples with increasing copper loading to 1, 5, and 10%, respectively). With increasing copper loading the band for mononitrosyl species on Cu^{2+} ions shifts from about 1890 to 1878 cm^{-1} and correspondingly the band for mononitrosyl on Cu^+ ions shifts to lower frequencies (from 1786 to 1767 cm^{-1}). This indicates a progressive decrease in the electron acceptor ability of copper ions as copper loading increases due to an increased lateral interaction between copper ions with formation of direct oxygen bonds between copper ions. In bulk $CuAl_2O_4$ (spectrum d of Fig. 7C) the coordinated mononitrosyl species is found at 1876 cm^{-1} which corresponds to the frequency of gaseous NO, indicating a nearly zero ionic character of the bond. On the contrary, the spectra after different times of evacuation (spectra b–c of Figs. 7B, 7C, and 7D) do not show a marked difference in the stability of the nitrosyl complexes.

Marked differences are also observed in the region below 1700 cm^{-1} for the oxidized nitrogen oxide species. An intense band due to nitrite–nitrate species forms in the interaction with NO in the absence of gaseous oxygen and its intensity is proportional to the copper loading on alumina (see spectra a of Figs. 7C, 7B, and 7D for CuAl-1, CuAl-5, and CuAl-10, respectively). In addition, the nature of these species also changes as a function of copper loading. On CuAl-1 (Fig. 7C), together with a broad absorption band at around 1600 cm^{-1} with a distinct peak at 1614 cm^{-1}, bands are observed at 1226, 1322, 1350, and 1468 cm^{-1}. These bands are in good agreement

with those observed on pure alumina (Fig. 7A) and thus can be attributed to the same species formed on a free alumina surface, since the copper coverage is much less than that necessary for complete monolayer formation [around 4.2 as wt% of CuO according to Friedman *et al.* (17)]. The band at 1614 cm^{-1} can be attributed, on the contrary, to the asymmetric stretching frequency of a bridging nitrate tentatively on a copper and aluminium ion [Al–O–NO–O–Cu] (20, 42). The second component of the split doubly degenerate asymmetric stretching mode is expected at about 1170–1220 cm^{-1} in agreement with the broader band observed in this range of frequencies on CuAl-1 (Fig. 7C) as compared to alumina (Fig. 7A). Symmetric modes for nitrate ions are expected below 1100 cm^{-1}, where the intense bands of skeletal vibrations of the catalyst, in our case, prevent analysis.

In CuAl-5 (Fig. 7B), in comparison to CuAl-1, the bands of nitrite ions linked to aluminium ions disappear, suggesting that almost the entire surface of alumina is modified by copper ions. Two clear bands at about 1250 and 1292 cm^{-1} with a weaker shoulder at about 1220 cm^{-1} can be observed in the 1200–1300 cm^{-1} region as well as a broad structured absorption band in the 1400–1650 cm^{-1} region with distinct maxima at 1500 and 1620 cm^{-1} (spectra a–c of Fig. 7B). It should be noted that for "oxidized" CuAl-5 a slightly different spectrum is observed in this region (spectrum d of Fig. 7B) with a maximum at 1568 cm^{-1}. The spectra suggest the presence of monodentate (1500 cm^{-1}) and bidentate (1568 cm^{-1}) species on Cu ions, in addition to the nitrate ion bridging copper and aluminium ions as for CuAl-1. The second ν_3 stretching frequency for both these nitrate species is expected in the 1200–1300 cm^{-1} region in agreement with the spectrum observed. Both these nitrate species are present, but their relative amounts depend on the sample pretreatment. The oxidizing pretreatment favors the relative formation of bidentate nitrates with respect to monodentate, with a parallel increase in the 1250 cm^{-1} component with respect to 1292 cm^{-1} component.

In CuAl-10 (Fig. 7D) similar nitrate species are detected, but the relative amount of the bidentate nitrate species increases and the component at 1620 cm^{-1} assigned to a nitrate species bridging copper and aluminium sites is absent. In agreement, it should be noted that this component is clearly absent in bulk $CuAl_2O_4$ (spectrum d of Fig. 7C).

Increases in the copper loading on alumina, therefore, lead to a series of changes in the nature of adsorbed nitrogen oxides species after interaction with NO at 300°C: (i) the ionic character of mononitrosyl adsorbed species progressively decreases, (ii) nitrite species on free alumina disappear, (iii) the amount of nitrate species formed in the absence of gaseous oxygen increases considerably, and (iv) the nature of the nitrate species also changes with disappearance of nitrate species bridging copper and aluminium ions and formation of mono- and bidentate nitrate ions on copper, the latter predominating for the higher copper loadings.

c. NO and NH_3 coadsorption. Chemisorbed ammonia and nitrite–nitrate species show bands in the same region and therefore it is difficult to deduce unequivocal information on the reaction mechanism from these experiments; even so, some useful data can be obtained. Tests were carried out with both (i) preadsorption of ammonia, evacuation, and consecutive interaction with NO and (ii) preadsorption of NO, evacuation, and consecutive interaction with ammonia. In the latter case, however, only the bands of chemisorbed ammonia were observed, even when small amounts of ammonia were employed. This can be due to a rapid disappearance of adsorbed nitrate species in contact with ammonia or to the high intensity of the bands for ammonia which cover those of nitrate species making it difficult to obtain reliable information. Better results were obtained, on the contrary, when NO was put in contact with catalysts on which ammonia had been preadsorbed.

Figure 8 shows the spectra obtained after contact at 150°C of 20 torr NO with CuAl-1 (spectrum a) after 90 min, with CuAl-5 after 10 and 20 min (spectra b and c) and with CuAl-10 for 10 min (spectrum d). On all samples, ammonia was preadsorbed at 150°C and then gaseous species were removed by evacuation at the same temperature.

In all samples the mononitrosyl species coordinated on Cu^{2+} can be observed. The frequency of this species shifts from 1890 to 1876 cm^{-1} as copper loading increases similarly to that discussed above. For the CuAl-1 sample, this band is much broader than that observed for only NO absorption, possibly due to a modification of coordination environment for copper due to chemisorbed ammonia. Mononitrosyl coordinated on Cu^{+} ions can be observed, on the contrary, only on CuAl-10.

The spectrum obtained on CuAl-1 below 1700 cm^{-1} can be interpreted as the overlapping of the spectra obtained by separated absorption of ammonia and NO. Ammonia is present as both coordinated ammonia (1618 and 1270 cm^{-1}) and ammonium ions (1470 and 1680 cm^{-1}). NO is present as linearly (1470 and 1350 cm^{-1}) or bridging (1230 cm^{-1}) coordinated nitrite ion, whereas the nitrate ion absorption near 1600 cm^{-1} is covered by that of ammonia. However, with respect to the overlap of the two spectra obtained from separate absorptions, it could be noted that an additional relatively intense band is present at 1394 cm^{-1} and that the intensity of the bands at 1470 and 1680 cm^{-1} is much stronger than that obtained in the case of ammonia adsorption alone on CuAl-1. The latter evidence tentatively suggests that coordinated ammonia partially reacted with NO forming N_2 and H_2O and thus generating

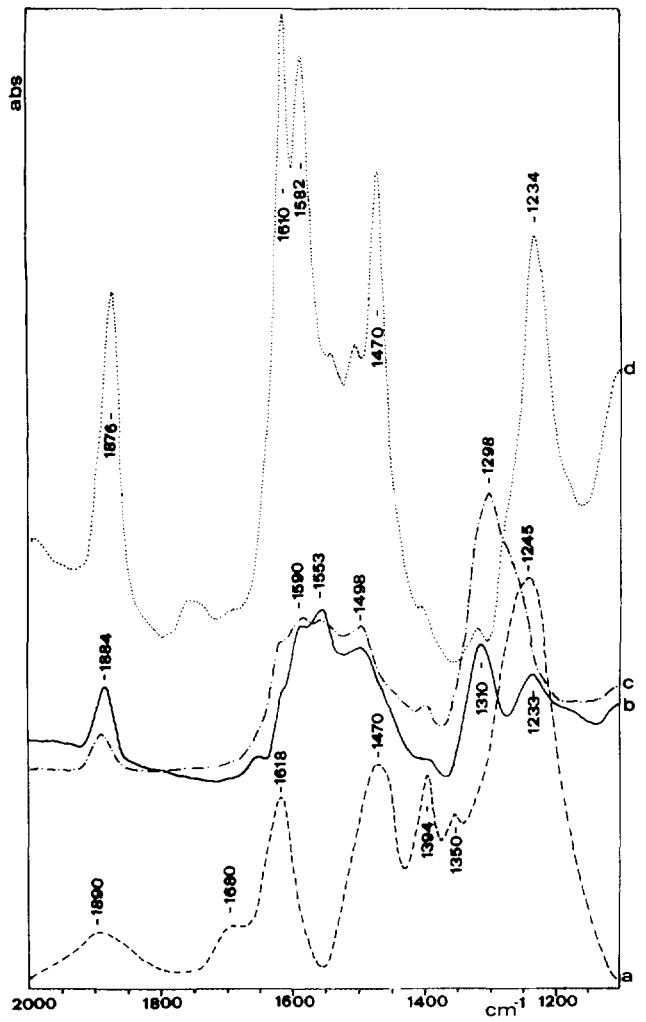

FIG. 8. Infrared spectra of ammonia and NO coadsorption: preadsorption of ammonia [contact of ammonia (40 Torr at 150°C for 1 h), followed by evacuation for 2 h] and then contact of NO (20 Torr at 150°C). (a) CuAl-1 after 90 min contact with NO, (b) CuAl-5 after 10 min and (c) 20 min of contact with NO, (d) CuAl-10 after 10 min contact with NO.

new Brønsted sites to which the ammonia shifted, since ammonia is more stable on the Brønsted sites. This suggests that ammonium ions may be present in significant amounts during the catalytic reaction and that coordinated ammonia apparently reacts faster. The bands at 1394 cm^{-1}, on the contrary, may be indicative of the formation of a nearly symmetrical nitrate ion such as that expected for ammonium nitrate or N_2O_4 dimers for which, however, a second intense band near 1720 cm^{-1} also is expected (42). The former interpretation of the presence of ammonium nitrate seems more reasonable.

On CuAl-5 (spectra b and c) and CuAl-10 (spectrum d) the spectra obtained by NO contact with preadsorbed ammonia can also be interpreted as the overlap of the spectra of separate ammonia adsorption and NO contact, but a modification in the expected intensities of some bands is observed, particularly for CuAl-10. The bands at 1470 cm^{-1} (ammonium ion) and 1610 cm^{-1} (coordinated ammonia) are very intense, but for the former the component at about 1660–1680 cm^{-1} is absent (or very weak). This band is IR inactive, but usually becomes visible due to the lowering of the symmetry of ammonium ions on the surface. In CuAl-5 (spectrum b) a weak band is present at about 1660 cm^{-1}. This suggests that ammonium ions can be present on CuAl-5 and CuAl-10, but their amount progressively decreases with increasing copper loading.

The band at 1610 cm^{-1} suggests the presence of coordinated ammonia, but since the symmetric deformation mode at about 1270 cm^{-1} is absent *or very weak* (see spectrum d of Fig. 6B), coordinated ammonia is present in limited amounts. The intense band at 1610 cm^{-1} may be thus attributed to the overlapping of the ammonia band and of the band of a nitrogen oxide species, possibly a bridging nitrate ion. Interestingly the latter species does not form on CuAl-10 in the absence of preadsorbed ammonia (compare spectrum d of Fig. 8 with spectrum a of Fig. 7D). Also the amount of the bidentate nitrate species becomes predominant with respect to that of the monodentate species mainly formed during NO interaction in the absence of preadsorbed ammonia. These data thus suggest that the nature of chemisorbed nitrate species is influenced by the presence of adsorbed ammonia. The presence of a band at about 1390 cm^{-1} in all the samples suggests, in addition, the possible formation of ammonium nitrate by reaction between coordinated species.

Additional information on the reaction mechanism can be obtained when, after ammonia preadsorption and contact with NO at lower temperature, the catalyst is treated under vacuum at different temperatures. Summarized in Fig. 9 are the experiments on CuAl-5 after preadsorption of ammonia at 150°C, evacuation at the same temperature, contact with NO at 100°C for 30 min, and subsequent evacuation at the same temperature (spectrum a), at 200°C (spectrum b) and 300°C (spectrum c). Spectrum d of Fig. 9 reports, on the other hand, the adsorbed species obtained after ammonia preadsorption as before, but after contact with NO at RT and evacuation at the same temperature. In this case, a strong absorption band centered at 1485 cm^{-1} with a second intense band at 1300 cm^{-1} develop, in addition to the bands at 1620 and 1250 cm^{-1} of coordinated ammonia. Tentatively, this species can be attributed to a bridging pseudo-nitrite species on copper ions [Cu–NO–O–Cu]. This species decreases considerably by interaction of NO at 100°C or higher temperatures (spectra a–c), but new bands form at 1590 and 1565 cm^{-1} due to the oxidation of pseudo-nitrite ions to nitrate ions. No significant differences are observed by evacuation at 100 and 200°C, but after evacuation at 300°C only two bands

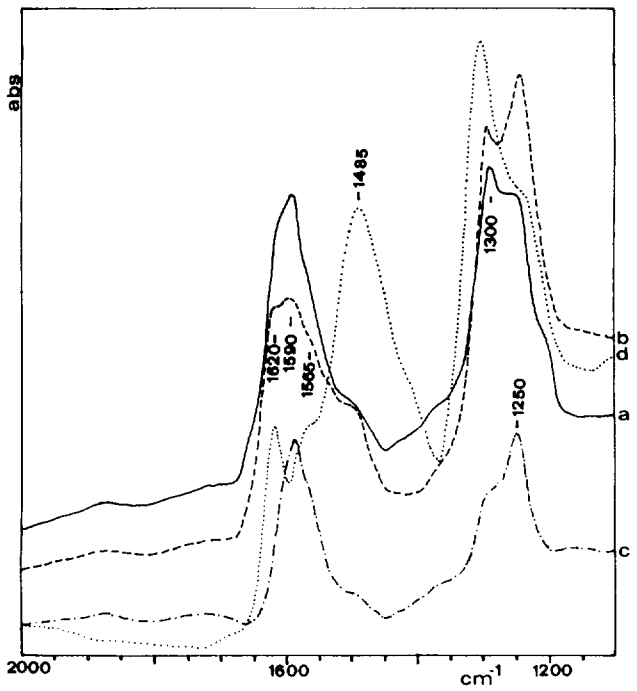

FIG. 9. Infrared spectra of ammonia and NO coadsorption on CuAl-5: preadsorption of ammonia [contact of ammonia (20 Torr at 150°C for 1 h), followed by evacuation for 2h] and then contact of NO (10 Torr at 100°C) for 30 min, and subsequent evacuation for 20 min at increasing temperatures: (a) 100°C, (b) 200°C and (c) 300°C. (d) Spectrum obtained by adsorption of NH_3 (20 Torr at RT), evacuation at RT for 5 min and subsequent contact of NO (10 Torr at RT for 15 min).

centered at 1590 and 1250 cm^{-1} remain due to a bridging nitrate species. This indicates that at higher temperature, nitrate ions react with chemisorbed ammonia to form N_2 and H_2O and further suggests that mono- and bidentate nitrate ions may react faster than bridging species. This agrees, on the other hand, with the change in the relative intensities of nitrate species on CuAl-10 in the presence or absence of chemisorbed ammonia discussed above.

XRD and UV–Visible Diffuse Reflectance Data

The amount of crystalline CuO detected as a function of the copper loading was detected by quantitative X-ray diffraction analysis using calibrated amounts of KBr as an internal standard and a mechanical mixture of 10 wt% CuO and γ-Al_2O_3 as the reference. Weak diffraction lines corresponding to crystalline CuO are detected only for samples with a copper loading above approximately 8%. Taking into account that the surface area of these samples is about 115 m^2g^{-1}, this value is significantly higher than that indicated in the past (>4 wt% for a 100 m^2g^{-1} alumina) by Friedman *et al.* (17), for example, as the limit for the detection of crystalline CuO on γ-Al_2O_3. For the CuAl-10 sample, only about 10% of the copper is detected as crystalline CuO.

UV–visible diffuse reflectance spectra of the samples as a function of the copper loading are shown in Fig. 10. Above 5% of copper loading, the spectra do not significantly differ from that for CuAl-5. According to previous results (11, 13, 17, 43) copper-on-alumina samples are characterized by an absorption band near 14,000 cm^{-1} and a stronger absorption near 35,000–40,000 cm^{-1}. The first can be attributed to the $^2E_g \rightarrow {}^2T_{2g}$ spin-allowed transition of Cu^{2+} ions in the distorted octahedral environment of surface alumina sites with a spinel-type structure, whereas the intense bands above 35,000 cm^{-1} are oxygen to copper charge-transfer bands. However, a more careful analysis of the reflectance spectra shows some minor, but significant, changes as a function of the increasing copper loading. The lower frequency band shifts from 13,000 to 15,000 cm^{-1} in going from CuAl-1 to CuAl-5 and a weak shoulder develops, centered at about 21,000 cm^{-1} (inset of Fig. 10). These effects can be attributed to an increased lateral interaction of copper ions on the alumina matrix which decreases the symmetry of the octahedral sites, in agreement with a similar shift observed upon coordination of ammonia on Cu^{2+} sites of copper-on-alumina (17) and the presence of interband transitions in semiconductor CuO above 20,000 cm^{-1}.

DISCUSSION

The analysis of the reactivity in NO reduction to N_2 by $NH_3 + O_2$ and NH_3 oxidation to N_2 as a function of the copper loading shows two peculiar aspects of the catalytic behavior of these catalysts:

(1) The rate of NO or NH_3 depletion increases as the amount of copper in the catalyst increases, but the specific rate per mole of copper decreases in the first case and is nearly constant in the second.

(2) The rate of oxidation of ammonia to N_2 is significantly higher in the absence of NO than in its presence. This last fact is valid for all copper-on-alumina samples, but is especially evident for those with the higher copper contents.

Up to a copper loading of about 8%, XRD analysis does not evidence any crystalline copper oxide. UV–visible diffuse reflectance spectra (Fig. 10) suggest that paracrystalline copper oxide may be present for lower copper loadings (around 5–8% range). However, the reactivity data (Fig. 3) show that the main change in the specific activity in the SCR reaction occurs with a copper loading below 5% (expressed as CuO). Therefore, the formation of copper microcrystallites with a consequent decrease in the number of available surface copper sites does not appear to be a reasonable explanation for the change of specific activity.

ESR data (Fig. 4) show that clustered copper ions exist together with isolated copper ions. With increasing copper

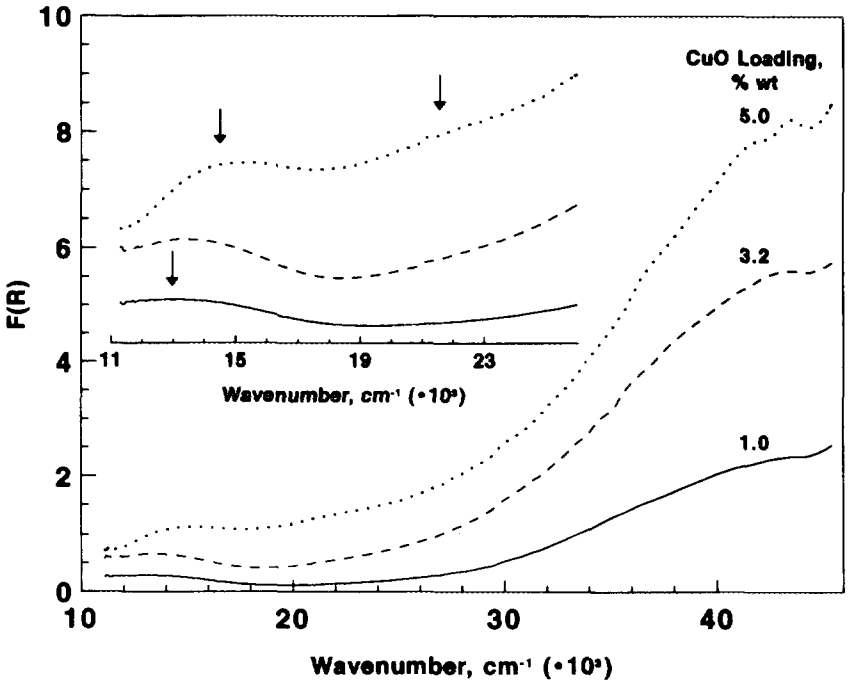

FIG. 10. UV–visible diffuse reflectance spectra as a function of the copper loading of copper-on-alumina samples.

content, the clustered copper ions become predominant, but they also are present in a significantly large proportion even for a very low copper content (0.1%). It is interesting to observe that the unstructured ESR signal attributed to clustered copper ions broadens slightly as the copper content increases from 0.1 to 5% (Fig. 4) due to the increased dipolar interaction between adjacent copper ions. However, it must be taken into account that crystallites of CuO escape ESR detection and that it is generally accepted that only a fraction of the whole Cu^{2+} in Cu^{2+}/Al_2O_3 is ESR visible (27, 28). According to the Knözinger–Ratnasamy model for the surface structure of γ-Al_2O_3 (37), copper ions on the C-layer locate in the defects of the spinel-type alumina structure forming rows of copper ions on capping oxygens. The expected distance between copper ions along the row is around 3–4 Å, whereas between adjacent copper rows the distance is larger than that necessary to have dipolar broadening. Similarly, the distance between copper ions in the ideal localization in surface defects of the D-layer, is higher than that necessary to induce broadening of the ESR signal of Cu^{2+}. According to this surface model, it is thus possible to attribute the ESR signal of clustered copper ions to copper ions with adjacent Cu^{2+} in rows on the C-layer and the structured ESR signal to isolated copper sites on the D-layer. The latter form preferentially at the lower copper loadings, whereas the former progressively build up with increasing copper content. This effect influences, on the other hand, the electronic properties (long-range electron transfer between acceptor sites in columns) with an expected decrease in the localization of charge on a single copper ion. Accordingly, UV–visible diffuse reflectance spectra (Fig. 10) show a progressive shift in the maximum of the $^2E_g \rightarrow {}^2T_{2g}$ band for Cu^{2+} ions in distorted octahedral coordination. IR data for NO in contact with these catalysts (Figs. 7 and 8) show that the mononitrosyl species shifts from higher to lower frequencies (from 1890 to 1878 cm^{-1}) with increasing copper loading due to the decrease in electron back donation to π^* orbitals of NO.

Spectroscopic data are thus in agreement with the surface model discussed above which suggests a progressive change in the electronic properties of copper ions. This also implies a change in their redox properties. In agreement, ESR data indicate a dependence of the intensity of the ESR signal upon reduction or reoxidation on the copper content. In summary, up to a copper loading of approximately 5% (expressed as CuO), a progressive change in the electronic characteristics of the copper ions can be expected together with the formation of microcrystallites and then crystallites of CuO at the higher loadings. This can well explain the observed dependence of the specific rate of NO depletion on the copper loading (Fig. 3). However, the independence of the specific rate of NH_3 depletion and the inhibition by NO of the rate of ammonia direct oxidation to N_2 cannot be rationalized on the basis of only this surface model of copper-on-alumina catalysts.

On the other hand, it seems unlikely that the modification by NO of the rate of the side reaction of ammonia

oxidation may be attributed to a kinetic effect due to the faster and preferential reaction of chemisorbed ammonia with NO that reduces the possibility of direct oxidation of ammonia to N_2. In this case, a significant increase in the rate of ammonia depletion is expected when NO is present, differently from what is experimentally observed (see, in particular, the results for the higher copper loading in Fig. 2b). In addition, a kinetic effect on the selectivity of the reaction of ammonia conversion is expected to be independent of the copper loading, differently from the observation of the different dependence of the specific rate constants of NO and NH_3 depletion from the copper loading (Fig. 3). Finally, the kinetic effect is not in accordance with the results of infrared characterization of chemisorbed species (see below). It is thus necessary to analyze the possible mechanism of NO and NH_3 conversion and the nature of chemisorbed species present during the catalytic reaction.

IR data (Fig. 6) show that ammonia is preferentially adsorbed as coordinated ammonia on Cu^{2+}, but copper–amino $[Cu(NH_3)_n]^{2+}$ complexes cannot be ruled out since their IR spectra nearly coincide with that for the mono-amino complexes (44). ESR evidence (Fig. 5c) also indicates the formation of copper-amino complexes. IR data also show that adsorbed ammonia is quickly converted to N_2 in the presence of gaseous oxygen at 300°C and copper ions catalyze this reaction (Fig. 6A). Coordinatively adsorbed ammonia apparently reacts faster than ammonium ions with oxygen. In addition, IR data also tentatively suggest that ammonia species produced by heterolytic ammonia splitting at higher temperature react even faster. It may thus be suggested that the reaction of ammonia oxidation to N_2 involves the heterolytic splitting of coordinatively adsorbed ammonia on Cu^{2+} ions to form $Cu–NH_2$ and –OH groups. These react with gaseous oxygen or an oxygen species activated by a nearlying copper ion forming a Ni · species and H_2O, the former migrating on the surface to recombine with another N · species to form N_2. Chemisorbed ammonia may also migrate to these generated Brønsted sites, as shown by IR data (Fig. 6), since ammonia is more stable on Brønsted sites. The higher relative amount of ammonium ions with respect to coordinatively adsorbed ammonia was also observed in NO and NH_3 reactive coadsorption experiments (Figs. 8 and 9). These data show that ammonium ions are present in significant amounts during the catalytic reaction and may thus play a role in the reaction mechanism.

NH_3 and NO coadsorption experiments show that (i) nitrate species react with adsorbed ammonia to form species not detectable by IR analysis (presumably N_2 or N_2O, the latter desorbing at the temperatures of the coadsorption experiments) and (ii) ammonium nitrate forms, although in small amounts. It is well known that the thermal transformation of NH_4NO_3 leads to the formation of N_2O, this being one of the industrial production methods of N_2O. It is also known that copper ions catalyze the decomposition of N_2O to N_2 and O_2 (45). Both these reactions occur at temperatures analogous to those used in the catalytic tests. The formation of ammonium nitrate on copper-on-alumina and the further transformation of this intermediate can thus explain the formation of N_2O observed during the catalytic tests (Fig. 1). On the other hand, the IR data show that the amount of nitrate species formed in the absence of oxygen is not correlated with the relative intensity of the IR bands attributed to ammonium nitrate (Fig. 8). In addition, the selectivity to N_2O increases only slightly with decreasing space–velocity (Fig. 1b), in contrast with the hypothesis that the transformation of NO in the presence of $NH_3 + O_2$ occurs via the intermediate formation of ammonium nitrate. These data, on the contrary, suggest that this last pathway of NO conversion occurs during the catalytic reaction, but is only a secondary pathway responsible for the formation of the byproduct N_2O. In agreement with this interpretation, it should be noted that during the simultaneous conversion of SO_2 and NO in the presence of $NH_3 + O_2$ on these catalysts (9, 46, 47), ammonium bisulfate forms on the surface, enhancing the ammonium ions avilable for the reaction with surface nitrates, the formation of which is only slightly influenced by the contemporaneous formation of sulfate. This effect leads to an enhanced formation of N_2O when SO_2 is cofed together with NO, NH_3, and O_2.

The formation of nitrate species and their high stability (reduced rate of further transformation), on the other hand, can well explain the observed inhibition of the side reaction of ammonia oxidation, because copper sites remain blocked by these species. The easier removal of chemisorbed mononitrosyl species by evacuation (Fig. 7) as compared to the stronger interaction of chemisorbed ammonia (Fig. 6) in fact indicates that ammonia replaces coordinated NO on Cu^{2+} sites, in contrast with the hypothesis that a strong NO coordination on Cu^{2+} may prevent the ammonia chemisorption and activation for the side reaction of oxidation to N_2. The inhibition of this side reaction derives, in contrast, from the formation of stable nitrate species. The formation of these nitrate species is not linearly correlated with the copper loading, but is significantly higher for the samples with the higher copper loadings (Fig. 7). The mechanism of inhibition by nitrate formation can thus explain why the specific activity in NH_3 oxidation is independent of the copper loading, but decreases in the case of the SCR reaction. At the same time, the site blockage by nitrate species, due to their low rate of transformation, also explains the inhibition of the side reaction of direct ammonia oxidation to N_2 in the presence of NO. This also indicates that the main reason for the change in the specific rate of NO depletion per mole of copper as a function of copper

loading on alumina is not a change in the specific turnover frequency of the active copper sites, but probably only a change in the number of free active copper sites (not blocked by nitrate species) during the catalytic reaction. A combination of these two effects, however, cannot be ruled out.

This mechanism of *in situ* modification of the surface reactivity of copper-on-alumina during the catalytic reaction also provides some indications regarding the reaction mechanism. Indeed, NO bonding as mononitrosyl species on Cu^{2+} was found to be rather weak, as confirmed also by ESR data (Fig. 5). Ammonia readily displaced the coordinated NO, if there was any. It was commented above that a reaction pathway involving the intermediate formation of ammonium nitrate is possible, but takes into account only a secondary pathway of NO transformation. The formation of nitrite species is possible at low temperatures (Figs. 7 and 9), but these species readily transform to nitrate species at higher temperature, especially when copper ions and oxygen are present. These data indicate that the intermediate formation of ammonium nitrite is possible, but also that it does not appear to be the more reasonable mechanism of reduction of NO to N_2 in the presence of $NH_3 + O_2$. The present data are more consistent with a reaction mechanism involving the heterolytic or homolytic splitting of NH_3 coordinated on Cu^{2+} sites and the reaction of NO (in the gas phase or weakly bound) with $Cu–NH_2$ to form N_2 and H_2O, similarly to what has been suggested for $V–TiO_2$ (48). The rapid partial transformation of coordinated ammonia species in contact with NO, suggested by the reactive coadsorption IR experiments (Fig. 8), is in agreement with this hypothesis for the reaction mechanism. On the other hand, the same experiments suggest that the mechanism of reaction involving ammonium ions and oxidized nitrogen oxide species is also possible. Competitive pathways of reaction are thus possible on copper-on-alumina catalysts and their relative importance may depend on the reaction conditions and catalyst characteristics. The predominance of one pathway over the other, however, cannot be singled out definitively on the basis of these results and further catalytic studies in nonstationary conditions are required.

ACKNOWLEDGMENT

The financial support from the national group on the "Structure and Reactivity of Surfaces" (MURST-40%) is gratefully acknowledged.

REFERENCES

1. Centi, G., Nigro, C., Perathoner, S., and Stella, G., *Catal. Today* 17, 103 (1993).
2. Iwamoto, M., and Hamada, H., *Catal. Today* **10,** 57 (1991).
3. Li, Y., and Armor, J. N., *Appl. Catal. B:Environment* **1,** 121 (1992).
4. Byrne, J. W., Chen, J. M., and Speronello, B. K., *Catal. Today* **13,** 33 (1992).
5. Li, Y., and Hall, W. K., *J. Phys. Chem.* **94,** 6145 (1990).
6. Centi, G., Perathoner, S., Kartheuser, B., Rohan, D., and Hodnett, B. K., *Appl. Catal. B:Environmental* **1,** 129 (1992).
7. Centi, G., Perathoner, S., Shioya, Y., and Ampo, M, *Res. Chem. Intermed.* **17,** 125 (1992).
8. Giamello, E., Murphy, D., Magnacca, G., Morterra, G., Shioya, Y., Nomura, T., and Ampo, M., *J. Catal.* **136,** 520 (1992).
9. Centi, G., Passarini, N., Perathoner, S., Riva, A., and Stella, G., *Ind. Eng. Chem. Res.* **31,** 1963 (1992).
10. Strohmeier, B. R., Leyden, D. E., Scott Field, R., and Hercules, D. M., *J. Catal.* **94,** 514 (1985).
11. Garbowski, E., and Primet, M., *J. Chem. Soc. Chem. Commun,* 11 (1991).
12. Marion, M. C., Garbowski, E., and Primet, M., *J. Chem. Soc. Faraday Trans.* **86,** 3027 (1990).
13. Lo Jacono, M., Cimino, A., and Inversi, M., *J. Catal.* **76,** 320 (1982).
14. Pepe, F., Angeletti, C., De Rossi, S., and Lo Jacono, M., *J. Catal.* **91,** 69 (1985).
15. Wolberg, A., and Roth, J. F., *J. Catal.* **15,** 250 (1969).
16. Hierl, R., Knözinger, H., and Urbach, H.-P., *J. Catal.* **69,** 479 (1981).
17. Friedman, R. M., Freeman, J. J., and Lytle, F. W., *J. Catal.* **55,** 10 (1978).
18. Laine, J., Severino, F., F., Lopez-Agudo, A., and Fierro, J. L. G., *J. Catal.* **129,** 297 (1991).
19. Fu, Y., Tian, Y., and Lin, P., *J. Catal.* **132,** 85 (1991).
20. Davydov, A. A. "Infrared Spectroscopy of Adsorbed Species on the Surface of Transition Metal Oxides," (Rochester, Ed.), Chap. 2, p. 71. Wiley, New York, 1990.
21. Deen, R., Scheltus, P. T., and Vries, G., *J. Catal.* **41,** 218 (1976).
22. Naccache, C., Che, M., and Ben Taarit, Y., *Chem. Phys. Lett.* **13,** 1091 (1972).
23. Gandhi, H. S., and Shelef, M., *J. Catal.* **28,** 1 (1973).
24. Hierl, R., Urbach, H.-P., and Knözinger, H., *J. Chem. Soc. Faraday Trans.* **88,** 355 (1992).
25. Otto, K., and Shelef, M., *J. Phys. Chem.* **76,** 37 (1972).
26. Marangozis, J., *Ind. Eng. Chem. Res.* **321,** 987 (1992).
27. Berger, P. A., and Roth, J. F., *J. Phys. Chem.* **71,** 4307 (1967).
28. Lumbeck, H., and Voitländer, J., *J. Catal.* **13,** 117 (1969).
29. Lunsford, J. H., *J. Catal.* **14,** 379 (1969).
30. Anpo, M., Nomura, T., Kitao, T., Giamello, E., Murphy, D., Che, M., and Fox, M. A., *Res. Chem. Intermed.* **15,** 225 (1991).
31. Naccache, C., Che, M., and Ben Taarit, Y., *Chem. Phys. Lett.* **13,** 109 (1972).
32. Chao, C. C., and Lunsford, J. H., *J. Phys. Chem.* **76,** 1546 (1972).
33. Vansant, E. F., and Linsford, H., *J. Phys. Chem.* **76,** 258 (1972).
34. Howard, J., and Nicol, J. M., *J. Chem. Soc. Faraday Trans. 1,* **85,** 1233 (1989).
35. Oates, M. D., and Lunsford, J. H., *J. Mol. Catal.* **9,** 91 (1980).
36. Tsyganenko, A. A., Pozdnyakov, D. V., and Filimonov, V. M., *J. Mol. Struct.* **29,** 299 (1975).
37. Knözinger, H., and Ratnasamy, P., *Catal. Rev. Sci. Eng.* **17,** 31 (1978).
38. Peri, J. B., *J. Phys. Chem.* **69,** 231 (1965).
39. Jobson, E., Baiker, A., and Wokaun, A., *J. Chem. Soc. Faraday Trans.* **86,** 1131 (1990).
40. Escalona Platero, E., Coluccia, S., and Zecchina, A., *J. Catal.* **103,** 270 (1987).
41. London, J. W., and Bell, A. T., *J. Catal.* **31,** 32 (1973).

42. Busca, G., and Lorenzelli, V., *J. Catal.* **72,** 303 (1981).
43. Freeman, J. J., and Friedman, R. T., *J. Chem. Soc. Faraday Trans. 1* **74,** 758 (1978).
44. Howard, J., and Nicol, J. M., *J. Chem. Soc. Faraday Trans. 1* **85,** 1233 (1989).
45. Riley, B. W., and Richmond, J. R., *Catal. Today* **17,** 277 (1993).
46. Centi, G., Passarini, N., Perathoner, S., and Stella, P., *in* "Proceedings, XIII Simposio Iberoamericano de Catalisis, Sergovia, Spain, 1992,"Vol. 1, p. 355.
47. Centi, G., Passarini, N., Perathoner, S., and Riva, A., *in* "New Frontiers in Catalysis" (L. Guzci, *et al.,* Eds.), p. 2677 Elsevier, Amsterdam 1993.
48. Ramis, G., Busca, G., Bregani, F., and Fozzatti, P., *Appl. Catal.* **64,** 259 (1990).